CrystEngComm

Accepted Manuscript

ROYAL SOCIETY OF CHEMISTRY

www.rsc.org/crystengcomm

Cite this: DOI: 10.1039/c0xx00000x

www.rsc.org/xxxxxx

ARTICLE TYPE

The enhanced photoelectrochemical performance of CdS quantum dots sensitized TiO_2 nanotube/ nanowire/ nanoparticle arrays hybrid nanostructures

Pin Lv, Haibin Yang,* Wuyou Fu,* Hairui Sun, Wenjiao Zhang, Meijing Li, Huizhen Yao, Yanli Chen, Yannan Mu, Lihua Yang, Jinwen Ma, Meiling Sun, Qian Li and Shi Su

This study aims at improving the photoelectrochemical performance mainly from two aspects: the increased number of heterojunctions and the advantages of nanotube/ nanowire/ nanoparticle arrays hybrid nanostructures. TiO_2 nanoparticles porous layer was sensitized by CdS quantum dots (QDs) ,and coated on the top of the material, hydrogen-treated TiO_2 nanotubes with nanowires, which was also sensitized by CdS QDs (This nanostructure defines as CdS/H:TTWP). CdS/H:TTWP was successfully fabricated by the methods of electrochemical anodization, successive ionic layer adsorption and reaction (SILAR) and sol-gel. The data of the photoelectrochemical (PEC) performance test shows that the photocurrent density of CdS/H:TTWP is 7.6 mA/cm^2 at -0.43V vs. Ag-AgCl under AM 1.5 G illuminations.

1. Introduction

In recent years, TiO_2 nanotubes has received extra attention because of their superior performances infields such as photocatalysis,[1] generation of hydrogen by water photoelectrolysis,[2,3] gas sensors,[4] tissue engineering scaffolds,[5,6] and dye-sensitized solar cells.[7,8] Compared with simple TiO_2 nanotubes, TiO_2 nanotubes with nanowires directly formed on top (denoted as TTW) has enlarged surface areas and can provide a direct pathway for photogenerated electron transfer, which accordingly leads to the enhancement of light harvesting and charge separation.[9] However, the wide band gap (3.2 eV) restricts the photoresponse of TiO_2 to only ultraviolet region with the wavelength below 380 nm the solar spectrum and depresses vastly utilization ratio of solar power. For extension of the optical absorption into the visible-light, various strategies have been designed, including doping TiO_2 with a metal or nonmetal and coupling it with organic dye or narrow band gap semiconductors.[10-14] In this report, we firstly combine nonmetal doping and narrow band gap semiconductors sensitization to extend the visible light absorption of TTW.

Some dopants such as nitrogen (N), carbon (C), and hydrogen (H) serve as electron donors to contribute to light absorption in the visible region and increase the electrical conductivity of the film.[15] In particular, the valence band edge of nonmetal (N, C)-incorporated TiO_2 is upshifted forming impurity states above the valence band or hybridizing with O 2p states to extend the absorption spectrum toward the visible light region. In contrast, the hydrogen-treated TiO_2 nanotubes (H:TTW) create vacancy sites, thus, forming donor states below the conduction band, which improves charge transport and light absorption similar to n-type doping, thereby enhancing PEC performance.[16] Therefore, hydrogen treatment based on a one-dimensional nanostructure photoanode can offer a synergetic effect with modifications of the intrinsic electrical properties of a TiO_2 material as well as the strong points of one-dimensional nanostructures. One-dimensional nanotubes were thermally treated in an H_2 atmosphere at 300 ^oC to demonstrate the decoupling effects in TiO_2, which substantially increased donor density and was closely correlated with electrical conductivity and charge transportation. Therefore, the photocurrent of hydrogen-treated TiO_2 significantly improved under full sunlight.[17,18]

In addition, the CdS quantumdots (QDs) sensitized the H:TTW film (CdS/H:TTW) by SILAR, because CdS nanoparticles are important narrow band gap semiconductor QDs and the photoresponse can be modulated in the visible-light spectrum by controlling their size.[19] Once the heterojunction structure of TiO_2/CdS formed, it not only improves the separation of electrons and holes, but also inhibits the recombination of the photogenerated hole-electron pairs effectively and prolongs the life of the photogenerated charge carriers.[20,21] But, more deposition cycles would cause conglomeration and growth of the CdS crystal nucleus, and the oversized CdS particles would lose the dominance as QDs (large QDs extinction coefficients and generating multiple electron-hole pairs), and moreover, excess CdS nanoparticles can act as potential barrier for charge transfer. Thus, the basis of doping and sensitization, we put a novel test to increasing the number of heterojunction to further promote the PEC activity. The idea is that CdS/H:TTW is coated with a thin porous layer of TiO_2 nanoparticles (denoted as H:TTWP), and continued to sensitize CdS QDs. The coated CdS/ TiO_2 nanoparticles (TNP) layer on top of the nanotubes had a larger surface areas to absorb visible light,[22-24] meanwhile the light can be scattered by the three-dimensional topography of the highly ordered CdS/H:TTW, thus allowing more light to be recycled by the heterojunction of CdS/TNP for additional photocurrent generation. This new mixed nanostructure combines the merits of nanotubes, nanowires and nanoparticles. Especially the nanowires are the tie for nanotubes and nanoparticles, such as a bridge to combine threes together.

2. Experimental section

2.1. Preparation of self-organized H:TTW array

Pure Ti foil (4 cm×3 cm, 0.4 mm thick, 99.9% purity) before anodization was cleaned in an ultrasonic bath with acetone, isopropanol and ethanol, followed by rinsing with deionized water and drying in a flow of N_2. The anodization was performed in a two-electrode configuration with titanium foil as the working electrode and graphite plate as the counter electrode under constant potential at room temperature. A direct current (dc) stabilized voltage and current power supply (WYJ60V3A, Pingguo instrumentation Co. Ltd. China) were employed as the voltage source to drive the anodization, and the distance between the two electrodes was 4 cm. Electrochemical anodization was performed at 40 V for 1 h in an electrolyte mixture containing 0.3 wt% NH_4F and 5.0 vol% deionized H_2O dissolved in the ethylene glycol. The as-anodic TTW was washed in ethanol for 5 min, dried under nitrogen gas, and transferred to a box furnace to anneal the as grown samples at 450 ^oC for 2 h under ambient air to improve the crystalline properties, followed by annealing in a mixture of H_2 and N_2 (4% of H_2) for an additional 30 min at temperature of 300 ^oC so the TTW were sustainable without any destruction of intrinsic structure.

2.2. Preparation of CdS/H:TTW array films

CdS QDs were assembled onto H:TTW by a successive ionic layer adsorption and reaction (SILAR) technique. The SILAR method is based on sequential reaction on the substrate surface by successive immersion of the substrate into separate cationic and anionic precursor solutions at room temperature. A two beaker SILAR system is used for deposition of CdS/H:TTW array. Firstly, the H:TTW films were soaked in ethanol solution which contains 0.5 M $Cd(NO_3)_2{\cdot}4H_2O$ for 10 min; following immersion, the films were rinsed with pure ethanol and dried at 150 ^oC for 10 min. Secondly, it was immersed into a 0.5 M $Na_2S{\cdot}9H_2O$ aqueous solution for another 10 min, rinsed with deionized water, and dried at 150 ^oC for 10 min. The entire procedure was termed as one cycle. Then, the samples were annealed at 300 ^oC for 1 h.

2.3. Preparation of CdS/H:TTWP array films

The TNP paste was synthesized by a sol-gel method. Tetrabutyl titanate ($Ti(OC_4H_9)_4$, TBOT) was selected as precursor, with anhydrous ethanol (C_2H_5OH, EtOH) as solvent, deionized water for hydrolysis, acetylacetone ($CH_3COCH_2COCH_3$, AcAc) as chelating agent. During synthesis, two different but equal parts of ethanol solutions were prepared. In the first part, TBOT was dissolved into EtOH, the solution was kept stirring for 30 min. The second part of the solution was then prepared by mixing the deionized water, EtOH and AcAc. These two solutions were then mixed and stirred for 2 h to achieve hydrolysis and condensation. The molar ratio was Materials TBOT: EtOH: H_2O: AcAc= 20: 30: 1: 2. The mixture was finally aged in a stable environment (with humidity lower than 30% and temperature of 20~25 ^oC) for 24 h.

The TNP paste was coated onto the surfaces of CdS/H:TTW using dip-coating method. The TNP past was obtained by dipping the CdS/H:TTW array in the precursor solution bath and pulled upwards with a constant speed of 4cm/min to keep uniform thickness of the film. The substrate coated with gel films were pretreated for 10 min in air at 300 ^oC. The effect of dip-coating times on the device performance had been carefully studied, the optimum number of times was found to be four porous layer and then were annealed at 450 ^oC for 2h. CdS QDs were assembled onto H:TTWP array by SILAR, mentioned previously in section 2.2. The detailed process of the CdS/H:TTWP is shown in Figure 1.

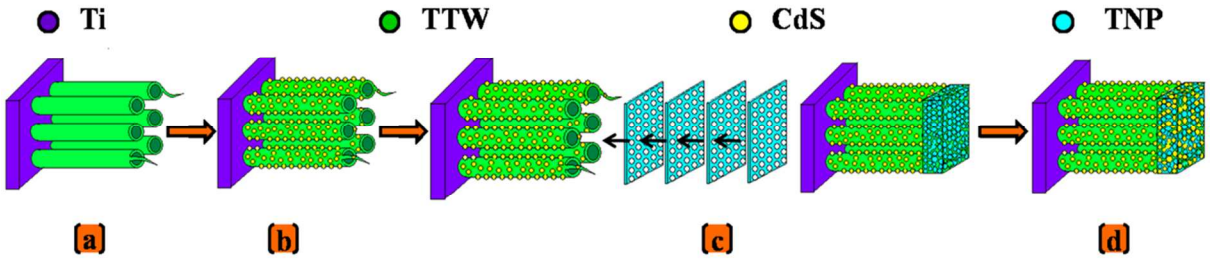

Figure 1 Schematic illustration of the formation process of the CdS/H:TTWP nanostructures. (a) TTWs, (b) CdS/H:TTW formed after hydrogen treatment and sensitization of CdS QDs, (c) TNP porous layer coating on CdS/H:TTW arrays was carried out using dip-coating method by four times, (d) CdS/H:TTWP

2.4. Characterization

A model JEOL JSM-6700F field-emission scanning electron microscope (FESEM) was used to characterize the morphologies of the samples. HRTEM images were obtained with a JEM-2100F high-resolution transmission microscope operating at 200 kV. Scanning TEM and energy-dispersive X-ray spectroscopy analyses (STEM-EDX) were taken by a FEI TECNAI F20 transmission electron microscope with an accelerating voltage of 200 kV. The crystal structure of the as-prepared films were characterized by a Rigaku D/max-ray diffractometer with Cu Karadiation (l= 1.5418 Å). Optical characterization of the films was performed using a UV-3150 double-beam spectrophotometer.

2.5. Photovoltaic measurements.

The photoelectrochemical properties were investigated using the conventional three-electrode system, which is made of quartz cell and linked with the electrochemical workstation (CH Instruments, model CHI601C). As-prepared film electrodes were used as the working electrode, a platinum mesh as the counter electrode and a saturated Ag/AgCl as the reference electrode. The electrolyte was composed of 0.25 M $Na_2S{\cdot}9H_2O$ and 0.35 M Na_2SO_3 aqueous solution. The electrolyte had a PH of about 12 and the solution potential was about −0.43 V versus Ag/AgCl. The CHI electrochemical workstation was used to measure dark and illuminated current at a scan rate of 10 mV/s. Sunlight was

simulated with a 500 W xenon lamp (Spectra Physics). The light intensity was calibrated by using a laser powermeter (BG26M92C, Midwest Group), equivalent to AM 1.5G light at 100 mW/cm^2.

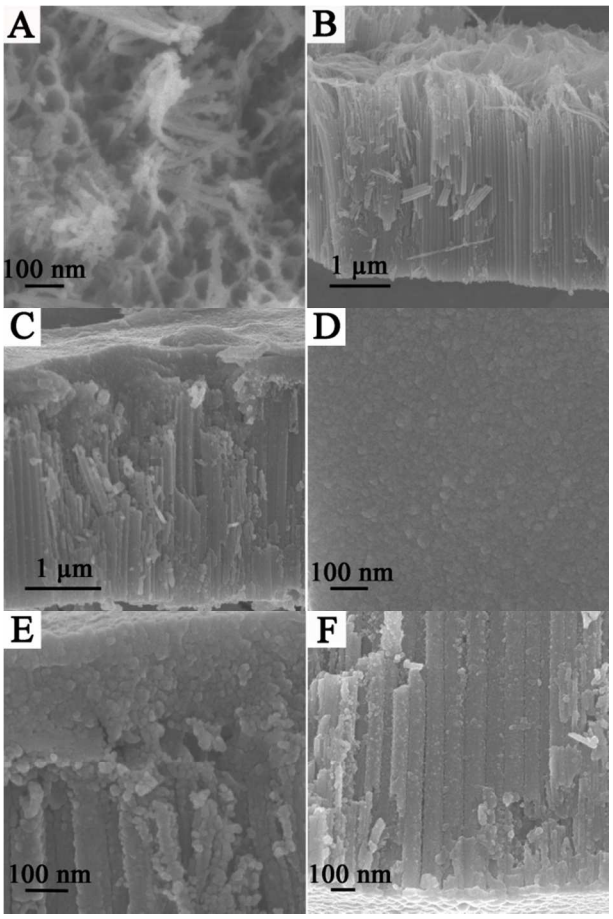

Figure 2 Field-emission scanning electron microscopy (FESEM) images: (A) and (B) are a top view and cross-section view of bare H:TTWs, respectively; (C) and (D) are a cross-section view and top view of CdS/H:TTWP electrode, respectively; (E) and (F) are the cross-section view of the top and bottom of CdS/H:TTWP electrode, respectively.

3. Results and discussion

3.1. SEM images

The FESEM images of the H:TTW and the CdS/H:TTWP array are shown in Figure 2. Figure 2A gives the top view of the H:TTW where the wires on top of the nanotube are so loosely arranged that some bare pore openings are exposed. Since the wires are formed by chemical dissolution of oxide at the top and there is no grain boundary between the tube and the wires, the H:TTW structure would inherit the advantages of both the nanotube and nanowire in charge separation, electronic transport, and light harvesting. Figure 2B shows cross-section FESEM images of the resulting samples. The H:TTW arrays is uniformly formed with tube lengths of 2.8μm and diameters of~100 nm, and there is no discrepancy in the top view and cross-section images were found between H:TTW and TTW. It powerfully proves that the crystal structure is not destroyed in the hydrogen treatment process. Figure 2C and D show side and top views of the CdS/H:TTWP array. Figure 2C shows the total thickness of this sample was around 3.2 μm (H:TTW layer ~ 2.8 μm and TNP layer ~ 0.4 μm). And Figure 2D shows few microcracks on the surface of the sample , on the contrary, the cracks are most likely to interrupt the continuous electron conduction and thus reduce the current density. From Figure 2E results , it can be deduced that the nanoparticles are in the 10nm to 20nm size range and are spherical in appearance. They are loosely agglomerated and thus can readily provide a high surface area. A porosity of the film is evidenced, highly favourable for CdS QDs adsorption. In addition, this Figure also shows that CdS/H:TTW and CdS/TNP blend well and grow together. The bottom of CdS/H:TTWP array with the rougher surfaces are observed as shown in Figure 2F, which reveals that CdS QDs have covered the entire surfaces of H:TTW.

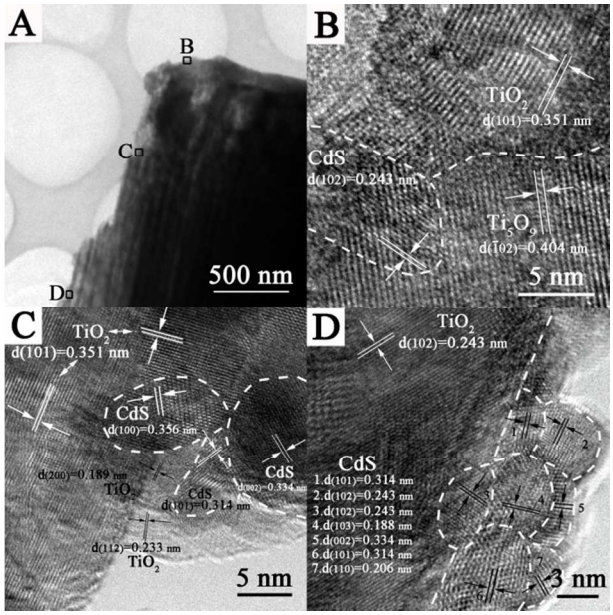

Figure 3 (A) TEM image of CdS/H:TTWP electrode; (B), (C), and (D) are HR-TEM images of a CdS/H:TTWP electrode in the CdS/TNP layer, the junctions between H:TTW and TNP, the bottom edge of CdS/H:TTW, respectively.

3.2. TEM and HRTEM observation

The transmission electron microscopy (TEM) image in Figure 3A is representative CdS/H:TTWP array. This image shows that the H:TTW and TNP can grow together well, which because their structure was not damaged through ultrasonic processing before the test. To get more detailed information of the crystalline structure of the CdS/H:TTWP, high-resolution transmission electron microscopy (HR-TEM) was carried out. The distinct lattice fringes in Figure 3B confirm the high crystalline nature of the CdS/TNP layer. The lattice fringe with a d-spacing of 0.351 nm belongs to the lattice fringe of the (101) plane of the anatase TiO_2 [JCPDS no. 86-1157], while the lattice fringe of 0.243 nm is assigned to the (102) plane of the hexagonal CdS [JCPDS no. 80-0006]. In addition, the lattice spacing of Ti_5O_9 is 0.404 nm, which matched with the ($\bar{1}$ 02) plane of triclinic Ti_5O_9 [JCPDS no. 71-627]. The formation of Ti_5O_9 in the internal CdS/TNP layer is caused by the weight and atomic percent oxygen of TiO_2 sol, and in a reducing atmosphere by the heated AcAc vapor.[25,26] The material of Ti_5O_9 also has been considered as potential electrodes for different uses, mainly due to their extremely high electrical

conductivity. In the CdS/TNP layer containing Ti_5O_9 can provide electronic transmission with a fast-track speed and reduce the resistance of the electrode. The larger crystallite appearing in the left and upper region of Figure 3C are identified to be TiO_2. The lattice spacing measured for these crystalline planes are 0.351 nm, both of corresponding to the (101) plane of anatase TiO_2, which are the nanotube and nanoparticle of TiO_2, respectively. Around the TiO_2 crystallite, fine crystallites with various orientations and lattice spacing are observed. By carefully measuring the lattice parameters and comparing with the data in JCPDS, the crystallites connecting to the TiO_2 are CdS. Thus, Figure 3C illustrates again H:TTW and TNP blend well and grow together, meanwhile the CdS QDs can penetrate into the bottom of porous TNP layer. Figure 3D shows the bottom edge of a nanotube, indicates high crystallinity of the nanotube, the larger crystallite appearing in the left region of the image is identified to be TiO_2. The lattice spacing measured for this crystalline planes is 0.243 nm, corresponding to the (102) plane of anatase TiO_2. The attached CdS QDs appear as randomly oriented crossed-fringe patterns on the bottom edge of the nanotube. HRTEM image also indicates that QDs deposited on TiO_2 nanotube have crystalline hexagonal structure, the observed 0.314 nm, 0.243 nm, 0.188 nm, 0.334 nm and 0.206 nm fringes of the QDs on the nanotube correspond to the (101), (102), (103), (002) and (110) planes, respectively, of the hexagonal phase of CdS.

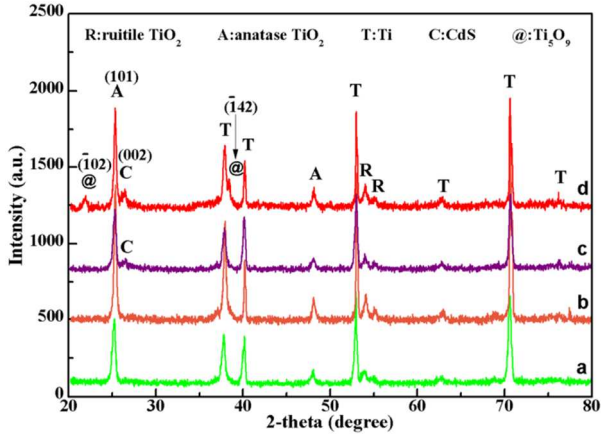

Figure 4 (A) XRD patterns of (a) TTWs, (b) H:TTWs, (c) CdS/H:TTWs and (d) CdS/H:TTWP electrode.

3.3. XRD spectra

Figure 4 shows the XRD patterns for the samples. The TTW arrays were readily crystallized in anatase and rutile phases after annealing in air at 450 ^oC for 2 h as shown in Figure 4a. As is shown in Figure 4b, there is no phase change after hydrogenation. But, it appeared that variations in the intensity of the peaks were strengthened. The sharp peaks reveal that the prepared H:TTW is well-crystallized, which is beneficial to the photoelectrode. The annealed CdS sensitized H:TTW arrays (Figure 4c) exhibit a new small peaks at 2θ of 26.65. This peak can be indexed to the (002) planes of thehexagonal CdS [JCPDS no. 80-0006], which is consistent with the HRTEM results above. Figure 4d shows the CdS/H:TTWP arrays exhibit new small peaks at 2θ of ca. 21.96, 38.61. These peaks can be indexed to the ($\bar{1}$ 02) and ($\bar{1}$ 42) planes of the triclinic-phase Ti_5O_9 [JCPDS No. 71-627], ($\bar{1}$ 02) planes is consistent with the HRTEM results above. Moreover, the intensity of anatase TiO_2 peaks at 2θ of 25.31 was strengthened (Figure 4d). It illustrates that the annealed TNP has major crystal planes of anatase (101) phase. The image of HRTEM can also be specified.

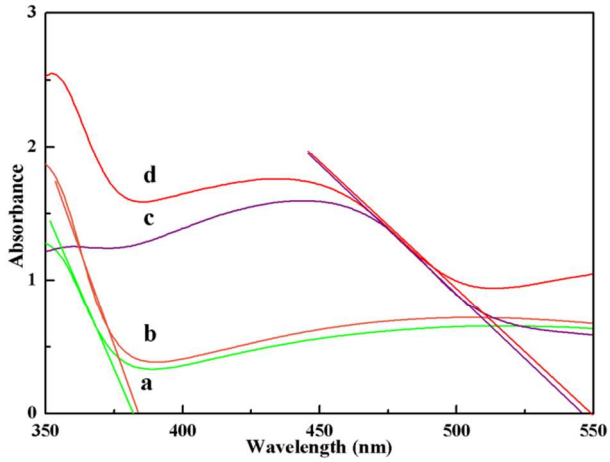

Figure 5 (A) XRD patterns of (a) TTWs, (b) H:TTWs, (c) CdS/H:TTWs and (d) CdS/H:TTWP electrode.

3.4. UV-vis absorption spectroscopy

The variation of UV vis spectra obtained in this work are shown in Figure 5, from which enhanced absorption of visible light by CdS/H:TTWP heterostructure can be confirmed. It can be seen that the maximum peak of the TTW film occurs at around 380 nm, and no significant absorbance for visible light can be seen because of its large energy gap (3.2 eV). However, the H:TTW films exhibited stronger absorbance from 350 to 385 nm and higher intensity than that of non-treated TTW film, it is probably due to the rapid creation of oxygen vacancies by hydrogen treatment, leading to a sub-band-gap transition corresponding to the excitation from the valence band to the impurity band. Accordingly, the band-to-band transition from the valence band to the conduction band as well as the sub-band-gap transition concurrently happened in the H:TTW films, whereas the band-to-band transition only occurred in the pure TTW film. In the UV vis spectra of CdS/H:TTW broader bands appear from 350 to 545 nm. This change indicates that the deposition of CdS QDs has significantly extended the photoresponse of H:TTW electrode in the visible light region. As known from the quantum-confinement effect, when the particle size is reduced to the quantum size, the number of atoms in a particle will enormously decrease and a larger interval between the energy level will emerge. Therefore, the energy level will change from quasi-continuous phase to split phase, and the energy gap will become so wide that the blue-shift in the absorption occurs. However, the samples of CdS/H:TTWP show that there is only slightly red-shift of band-edge to 550 nm because of the limitation of CdS energy gap (2.4 eV). But the absorption intensity increases obviously, by reason of the increasing number of heterojunctions. Meanwhile it indicates that the nanotubes, nanowires and nanoparticles mixed structure composites are conducive to the photoabsorption property. The enhanced ability to absorb visible-light of this type of CdS/H:TTWP makes them promising photovoltaic devices.

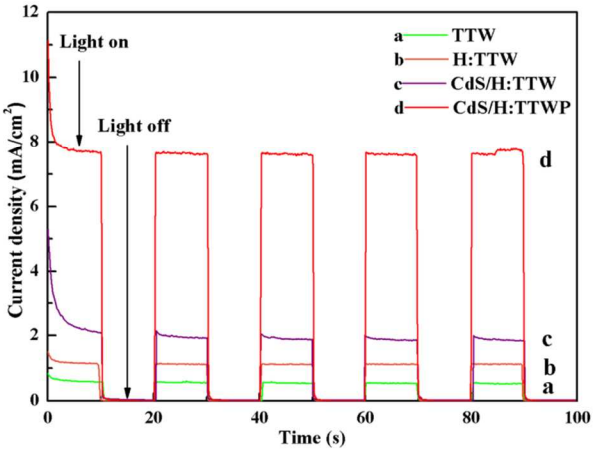

Figure 6 Photocurrent response of (a) TTWs, (b) H:TTWs, (c) CdS/H:TTWs and (d) CdS/H:TTWP under visible illumination at the bias voltage of 0 V.

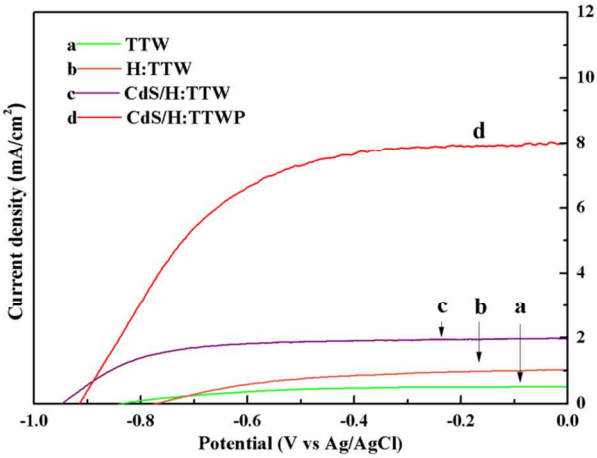

Figure 7 Photocurrent density-voltage curves of CdS/H:TTWP photoelectrodes: (a) TTWs, (b) H:TTWs, (c) CdS/H:TTWs and (d) CdS/H:TTWP. The active area was strictly kept within 1 cm^2, and the photoelectrodes were measured versus saturated Ag/AgCl electrode under simulated sunlight with an illumination intensity of 100 mW/cm^2 in 0.25 M $Na_2S{\cdot}9H_2O$ and 0.35 M Na_2SO_3 aqueous solution.

3.5. Photoelectrochemical behaviors

Photoelectrochemical measurements were performed in a three electrode electrochemical cell using the samples as the working electrode, a platinum coil as the counter electrode, and a reference of Ag-AgCl.[27-30] Figure 6 provides the photocurrent responses of the TTW under a 0 V bias vs.Ag/AgCl reference electrode. The bare TTW show very low photocurrent density under visible irradiation, and CdS/H:TTWP exhibit much higher photocurrent density than that of TTW. In Figure 7, the pristine TTW yielded a relatively low photocurrent density of 0.45 mA/cm^2, while the photocurrent density of H:TTW is 0.86 mA/cm^2 at -0.43V vs. Ag-AgCl. We conclude that the photocurrent density of H:TTW array were about two times higher than that of pure TTW array, demonstrating that H_2 treatment is a effective method to improve PEC performance. The comparison between the photoelectrochemical behavior of H:TTW and CdS/H:TTW electrodes confirms the superior performance of producing higher photocurrents for the latter over that of the former. It is obvious that the enhancement of the photoelectrochemical properties is a contribution of the CdS QDs sensitizer. The conduction band position of CdS is higher than that of TiO_2, once incident photons are absorbed by the CdS QDs, photoexcited electrons in the conduction band of CdS will quickly transfer into that of the TiO_2 to decrease its energy level. In this way, photoexcited electron-hole pairs are separated quickly and transported in their respective phases to the opposing electrodes, leading to enhancing photoelectrochemical activity. Thus, we draw a conclusion that the heterojunction of CdS/TiO_2 exists. Significantly, the photocurrent density of the CdS/H:TTW drastically increased after being coated with CdS/TNP layers, and achieved 7.6 mA/cm^2 at -0.43V vs. Ag-AgCl. The main reason is that the nanostructure of CdS/H:TTWP makes full use of nanotubes, nanowires and nanoparticles' advantages to recycle the light which scattered by the three-dimensional topography of the highly ordered CdS/H:TTW arrays. Consequently, the nanostucture improves the numbers of heterojunctions, and correspondingly increases the photocurrent density. The experiment data are favourable to proving this assertion as shown in Figure 8.

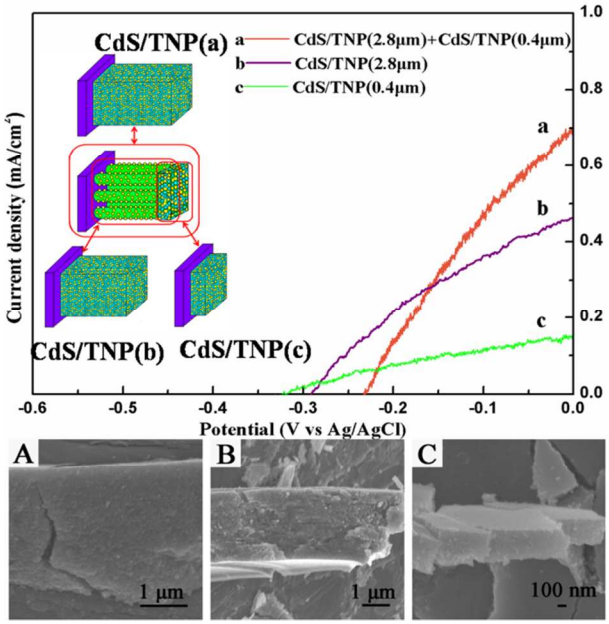

Figure 8 the photoelectrochemical performance of CdS/TNP layers with different thicknesses: (a) CdS/TNP(a) layers, (b) CdS/TNP(b) layers, (c) CdS/TNP(c) layers. The SEM images: (A) CdS/TNP(a) layers, (B) CdS/TNP(b) layers, (C) CdS/TNP(c) layers.

In Figure 8, the photoelectrochemical performance of CdS/TNP layers with different thicknesses have been shown. Firstly, CdS/TNP(a) layer and CdS/H:TTWP have the same thickness and deposition numbers of CdS, but the photocurrent of CdS/TNP(a) layer is 0.7 mA/cm^2, and that of CdS/H:TTWP is 11 times higher than the former. Viewed from the direct perspective, the difference between the both is that the former bottom is nanoparticles whereas the latter's is nanotubes. The large number of interface defects in the CdS/TNP(a) layer are the reason for electron annihilation during the transmission. By comparison, CdS/H:TTW, on the bottom of CdS/H:TTWP, will reduce the vertical interface defects. That's because the vertically aligned array of CdS/H:TTW can provide the continuous electrical conduction paths to Ti metal conductor underneath, which allow

more efficient electron transfer from the CdS/TNP layer and reduce the chance of charge recombination. It also means that the electrons may have longer lifetimes to contribute to the higher photocurrent. This explanation is reasonable, but not only.

Next, we set up the second comparison experiment, the CdS/TNP(b) layer and CdS/H:TTW have the same thickness and deposition numbers of CdS aiming at ruling out the factor of CdS/TNP layers. The result shows that the photocurrent of CdS/TNP(b) layer is 0.46 mA/cm^2, but that of CdS/H:TTW is only 4 times than the former's. Thus, the CdS/TNP layers also play an important role in photoelectric property. We can furtherly illustrate the importance of CdS/TNP layers by Figure 9. The distribution of element dots of Cd and S in the TNP layer are denser than that of in H:TTW array, so we can roughly judge that the heterojunctions of CdS/TNP is denser also. The main reason is that the surface effect of nanoparticles makes a highly concentration of active center to absorb amounts of CdS QDs. Accordingly, the increasing heterojunctions result in the improvment of photocurrent density.

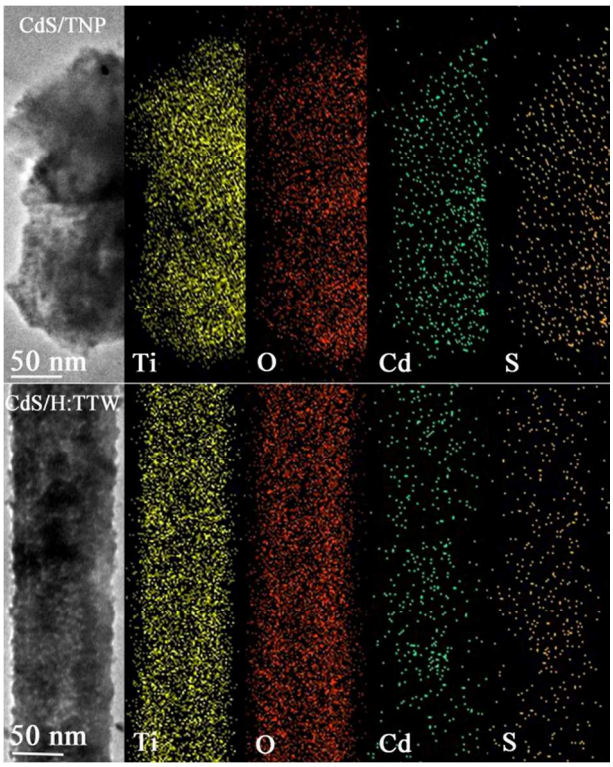

Figure 9 STEM images and the corresponding STEM-EDX elemental mappings of the sample (CdS/H:TTWP) are shown in two parts: CdS/TNP and CdS/H:TTW.

Based on the advantages of CdS/TNP layers, an idea may occurred to readers whether it has a better photoelectric property if the structure only has a thin CdS/TNP layer. During the experiment, CdS/TNP(c) has the same thickness and deposition numbers of CdS with the CdS/TNP layer which is on the top of CdS/H:TTWP. But the result of the photocurrent of CdS/TNP(c) is 0.15 mA/cm^2 only, and that of CdS/H:TTWP is 53 times higher. That because the CdS/TNP layer on the top of CdS/H:TTWP not only effectively increase the number of heterojunctions, but also recycle the light that scattered the three-dimensional topography of the highly ordered CdS/H:TTW arrays for additional photocurrent generation.

Hence, Only combining the nanotubes and nanoparticles together can the photoelectric properties be improved largely. Nanowires are the bridges between nanotubes and nanoparticles. Since the wires are formed by chemical dissolution (etching) of oxide at the top and there is no grain boundary between the tube and the wires. In addition, the wires are so loosely arranged on the top of the nanotube that they can enter into the inner of CdS/TNP layer easily, forming growth relationship. Therefore, nanotubes, nanowires and nanoparticles all play an important role in improving the photoelectrochemical performance, and also the morphologies of them exert their advantages fully in CdS/H:TTWP.

Conclusions

The CdS/H:TTWP film is successfully prepared by electrochemical anodization, SILAR and sol-gel methods. It improves the PEC performance in hydrogen treatment, sensitization of CdS QDs, morphology these three aspects. Firstly, the enhancement of PEC performance of hydrogen treatment of TTW films which would overcome the intrinsic material properties is mainly due to the increased donor density which lesded by the formation of oxygen vacancies in H:TTW samples. Secondly, the high PEC performance of CdS/H:TTW films can be attributed to both the improved light absorption in the visible wavelength range and the efficient separation of photo-generated electron-hole pairs. The last but the most important, the nanostructure of CdS/H:TTWP makes full use of nanotubes, nanowires and nanoparticles' advantages to recycle the light which scattered by the three-dimensional topography of the highly ordered CdS/H:TTW arrays. Consequently, the nanostucture improves the numbers of heterojunctions, and correspondingly increases the photocurrent density. The result of photogenerated photocurrent is 7.6 mA/cm^2 at -0.43V vs. Ag-AgCl under AM 1.5 G illuminations. These findings indicate that the CdS/H:TTWP film is a promising candidate material for PEC cells.

Acknowledgements

This work was financially supported by National Natural Science Foundation of China (No. 51272086) and the Technology Development Program of Jilin Province (Grant no. 20100417).

Notes and references

State Key Laboratory of Superhard Materials, Jilin University, Qianjin Street 2699, Changchun, 130012, People's Republic of China; Fax: +86 431 85168763; Tel: +86 431 85168763; E-mail: yanghb@jlu.edu.cn.

1 P. Lv, W. Y. Fu, H. B. Yang, H. R. Sun, Y. L. Chen, J. W. Ma, X. M. Zhou, L. C. Tian, W. J. Zhang, M. J. Li, H. Z. Yao and D. Wu, *CrystEngComm*, 2013, **15**, 7548.
2 R. Jayakumar, R. Ramachandran, V. V. Divyarani, K. P. Chennazhi, H. Tamura and S. V. Nair, *Int. J. Biol. Macromol.*, 2011, **48**, 336.
3 B. Zhou, M. Schulz, H. Y. Lin, S. I. Shah, J. H. Qu and C. P. Huang, *Appl. Catal. B*, 2009, **92**, 41.
4 M. Epifani, T. Andreu, R. Zamani, J. Arbiol, E. Comini, P. Siciliano, G. Faglia and J. R. Morante, *CrystEngComm*, 2011, **14**, 3882.
5 E. Alvarez-Guerra, A. Dominguez-Ramos and A. Irabien, *Chem. Eng. J.*, 2011, **170**, 7.
6 A. R. Boccaccini and J. J. Blaker, *J. Mater. Sci.*, 2006, **41**, 3999.
7 H. R. Bala, L. Jiang, W. Y. Fu, G. Y. Yuan, X. D. Wang and Z. R. Liu, *Appl. Phys. Lett.*, 2010, **97**, 153108.
8 H. J. Lee, J. Bang, J. Park, S. Kim and S. M. Park, *Chem. Mater.*, 2010,

22, 5636.
9 S. L. Cheng, W. Y. Fu, H. B. Yang, L. N. Zhang, J. W. Ma, H. Zhao, M. L. Sun and L. H. Yang, *J. Phys. Chem. C*, 2012, **116**, 2615.
10 S. Wang, J. M. Xu, H. L. Ding, S. S. Pan, Y. X. Zhang and G. H. Li, *CrystEngComm*, 2012, **14**, 7672.
11 X. L. Zhou, T. F. Zhou, J. C. Hu and J. L. Li, *CrystEngComm*, 2012, **14**, 5627.
12 M. M. Khan, S. A. Ansari, D. Pradhan, M. O. Ansari, D. H. Han, J. Lee and M. H. Cho, *J. Mater. Chem.* A, 2014, **2**, 637.
13 L. Zhang, Y. G. Li, Q. H. Zhang and H. Z. Wang, *CrystEngComm*, 2013, **15**, 5986.
14 M. Y. Zhang, C. L. Shao, J. B. Mu, Z.Y. Zhang, Z. C. Guo, P. Zhang and Y. C. Liu, *CrystEngComm*, 2012, **14**, 605.
15 X. Ma, Y. Wu, Y. Lu, J. Xu, Y. Wang, Y. Zhu, *J. Phys. Chem. C*, 2011, **115**, 16963.
16 L. X. Sang, Z. Y. Zhang, G. M. Bai, C. X. Du and C. F. Ma, *Int. J. Hydrogen Energy*, 2012, **37**, 854.
17 H. S. Kim and S. H. Kang, *Bull. Korean Chem. Soc.*, 2013, **34**, 7.
18 G. M. Wang, H. Y. Wang, Y. C. Ling, Y. C. Tang, X. Y. Yang, R. C. Fitzmorris, C. C. Wang, J. Z. Zhang and Y. Li, *Nano Lett.*, 2011, **11**, 3026.
19 H. Chen, W. Y. Fu, H. B. Yang, P. Sun, Y. Y. Zhang, L. R. Wang, W. Y. Zhao, X. M. Zhou, H. Zhao, Q. Jing, X. F. Qi and Y. X. Li, *Electrochim. Acta*, 2010, **56**, 919.
20 H. Kim, J. Kim, W. Kim and W. Choi, *J. Phys. Chem. C*, 2011, **115**, 9797.
21 X. M. Zhou, W. Y. Fu, H. B. Yang, Y. X. Li, Y. L. Chen, M. L. Sun, J. W. Ma, L. H. Yang, B. Zhao, L. C. Tian, *Electrochim. Acta*, 2013, **89**, 510.
22 L. B. Fen, T. K. Han, N. M. Nee, B. C. Ang, and M. R. Johan, *Appl. Surf. Sci.* 2011, **258**, 431.
23 W. J. Zhou, H. Liu, R. I. Boughton, G. j. Du, J. J. Lin, J. Y. Wang and D. Liu, *J. Mater. Chem.*, 2010, 20, 5993.
24 M. Dahl, S. Dang, J. B. Joo, Q. Zhang and Y. Yin, *CrystEngComm*, 2012, 14, 7680.
25 S. Lakkis and C. Schlenker, *PHYS REV B*, 1977, **16**, 6.
26 M. Canillas, E. Chinarro, M. Carballo-Vila, J. R. Jurado and B. Moreno, *J. Mater. Chem. B*, 2013, **1**, 6459.
27 Z. B. Shao, W. Zhu, Z. Li, Q. H. Yang, and G. Z. Wang, *J. Phys. Chem. C*, 2012, **116**, 2438.
28 J. S. Luo, L. Ma, T. C. He, C. F. Ng, S. J. Wang, H. D. Sun, and H. J. Fan, *J. Phys. Chem. C*, 2012, **116**, 11956.
29 H. Wang, Y. S. Bai, H. Zhang, Z. H. Zhang, J. H. Li and L. Guo, *J. Phys. Chem. C*, 2010, **114**, 1645.
30 W. Li, M. Y. Li, S. L. Xie, T. Zhai, M. H. Yu, C. L. Liang, X.W. Ouyang, X. H. Lu, H. H. Li and Y. X. Tong, *CrystEngComm*, 2013, **15**, 4212.